Int. J. Electrochem. Sci., 14 **(2019)** 10522 – 10530, doi: 10.20964/2019.11.47

International Journal of
ELECTROCHEMICAL
SCIENCE
www.electrochemsci.org

Short Communication

Characterization and Medium-Temperature Electrochemical Properties of $Ce_{0.8}Gd_{0.2}O_{2-\alpha}$-$K_2SO_4$-$Li_2SO_4$ Composite Electrolyte

Jie Liu[1], *Ruifeng Du*[1], *Tianhui Hu*[1], *Guangcheng Xi*[2], *Ruijuan Shi*[1,**], *Hongtao Wang*[1,*]

[1] School of Chemical and Material Engineering, Fuyang Normal University; Anhui Provincial Key Laboratory for Degradation and Monitoring of Pollution of the Environment, Fuyang 236037, China
[2] Chinese Academy of Inspection and Quarantine, Beijing 100176, China
[*]E-mail: hwang@fynu.edu.cn; rjshi@fynu.edu.cn

Received: 1 July 2019 / *Accepted:* 31 August 2019 / *Published:* 7 October 2019

In this study, $Ce_{0.8}Gd_{0.2}O_{2-\alpha}$ was synthesized by a sol-gel method. $Ce_{0.8}Gd_{0.2}O_{2-\alpha}$-$K_2SO_4$-$Li_2SO_4$ composite electrolyte was prepared by mixing $Ce_{0.8}Gd_{0.2}O_{2-\alpha}$ powder with binary sulphates. The structure of $Ce_{0.8}Gd_{0.2}O_{2-\alpha}$-$K_2SO_4$-$Li_2SO_4$ was characterized by Raman spectrometer. The morphology and phase composition of $Ce_{0.8}Gd_{0.2}O_{2-\alpha}$ and $Ce_{0.8}Gd_{0.2}O_{2-\alpha}$-$K_2SO_4$-$Li_2SO_4$ were characterized by scanning electron microscopy (SEM) and an X-ray diffraction (XRD). Arrhenius curves of $Ce_{0.8}Gd_{0.2}O_{2-\alpha}$ (1500 °C) and $Ce_{0.8}Gd_{0.2}O_{2-\alpha}$-$K_2SO_4$-$Li_2SO_4$ were tested in nitrogen at 400-700 °C. The maximum conductivity of $Ce_{0.8}Gd_{0.2}O_{2-\alpha}$-$K_2SO_4$-$Li_2SO_4$ reached 8.3×10^{-2} S·cm^{-1} at 700 °C.

Keywords: Composite; Fuel cell; CeO_2; Conductivity; Electrolyte

1. INTRODUCTION

Compared with other kinds of fuel cells, solid oxide fuel cells (SOFCs) not only have the advantages of high efficiency and environmental friendliness, but also have the following outstanding advantages: all-solid-state battery structures can avoid many problems caused by the use of liquid electrolytes [1-9]; the cost of electrode materials is reduced because of their low price; comprehensive utilization of heat to improve energy efficiency; fuel range is wide, etc. [10-16].

Doped CeO_2 has high ionic conductivity at medium temperature, which is considered to be one of the most important electrolyte materials for intermediate temperature (400–700 °C) solid oxide fuel cells (IT-SOFCs) [17-26]. Colet-Lagrille et al. synthesized $Mo_xCe_{1-x}O_{2-\delta}$ using a combustion method which had excellent catalytic activity for carbon gasification [25]. Liu et al. tested the content of acetone

using $Ce_{0.8}Gd_{0.2}O_{1.95}$ electrolyte [26]. The key to the development of IT-SOFCs lies in the exploration of new electrolyte materials.

In recent years, researchers have vigorously developed kinds of CeO_2-based composite electrolyte materials. Unlike traditional single-phase oxide electrolyte materials, these new materials are composed of doped CeO_2 and inorganic salt phases. During the operation of SOFCs, doped CeO_2 has the function of supporting the skeleton, while inorganic salts are distributed in the voids of doped CeO_2 grains in solid or melt state [27-35]. Fan et al. synthesized $Sm_{0.2}Ce_{0.8}O_2$-Na_2CO_3 composite electrolytes using one-step synthesis and applied them to SOFCs [33]. Therefore, it is of great theoretical and application value to study CeO_2-based composite electrolytes.

In this study, $Ce_{0.8}Gd_{0.2}O_{2-\alpha}$ was synthesized by a sol-gel method. $Ce_{0.8}Gd_{0.2}O_{2-\alpha}$-$K_2SO_4$-$Li_2SO_4$ composite electrolyte was prepared by mixing $Ce_{0.8}Gd_{0.2}O_{2-\alpha}$ powder with binary sulphates. $Ce_{0.8}Gd_{0.2}O_{2-\alpha}$ and $Ce_{0.8}Gd_{0.2}O_{2-\alpha}$-$K_2SO_4$-$Li_2SO_4$ were characterized and studied in terms of phase, morphology, conductivity and fuel cell performances at 400–700 °C.

2. EXPERIMENTAL

$Ce_{0.8}Gd_{0.2}O_{2-\alpha}$ was synthesized by a sol-gel method. Firstly, Gd_2O_3 (2.175 g) and $(NH_4)_2Ce(NO_3)_6$ (26.314 g) were completely dissolved with concentrated nitric acid and distilled water, respectively. Citric acid, as the complexing agent, was added and stirred until the consistency of the solution was about the same as that of honey. After baking at 100 °C for 24 h, the xerogel was burned for ashing. The ashes were sintered at 900 °C and 1500 °C for 5 h, respectively, to get $Ce_{0.8}Gd_{0.2}O_{2-\alpha}$. K_2SO_4-Li_2SO_4 was heat-treated in air for 1 h at 750 °C after full grinding with a molar ratio of 1:1. The obtained sulphate eutectic and $Ce_{0.8}Gd_{0.2}O_{2-\alpha}$ powders were mixed with the weight ratio of 2:8 and ground uniformly. $Ce_{0.8}Gd_{0.2}O_{2-\alpha}$-$K_2SO_4$-$Li_2SO_4$ composite electrolyte was obtained by heating the mixture for 1 h at 750 °C.

The gel was analyzed by thermogravimetry and differential scanning calorimetry (TG-DSC). The heating rate was 15 °C·min^{-1} and the temperature range was 50-900 °C. The phase compositions of $Ce_{0.8}Gd_{0.2}O_{2-\alpha}$ and $Ce_{0.8}Gd_{0.2}O_{2-\alpha}$-$K_2SO_4$-$Li_2SO_4$ were determined by X-ray diffraction (XRD). The structure of $Ce_{0.8}Gd_{0.2}O_{2-\alpha}$-$K_2SO_4$-$Li_2SO_4$ was further characterized by a Raman spectrometer. The morphology, grain size and density of $Ce_{0.8}Gd_{0.2}O_{2-\alpha}$ and $Ce_{0.8}Gd_{0.2}O_{2-\alpha}$-$K_2SO_4$-$Li_2SO_4$ were observed by scanning electron microscopy (SEM).

The $Ce_{0.8}Gd_{0.2}O_{2-\alpha}$ and $Ce_{0.8}Gd_{0.2}O_{2-\alpha}$-$K_2SO_4$-$Li_2SO_4$ were polished with sandpaper and coated with Pd-Ag slurry on both sides. The samples were dried and placed in an electric furnace. AC impedance spectroscopy was measured in a nitrogen atmosphere at 400-700 °C. The measurement frequency ranged from 1 to 10^5 Hz. Volt-ampere characteristic curves of the fuel cells were obtained by electrochemical workstations at 700 °C.

3. RESULTS AND DISCUSSION

The TG-DSC curve of the $Ce_{0.8}Gd_{0.2}O_{2-\alpha}$ gel from room temperature to 900 °C before and after ashing is shown in Fig. 1. In Fig. 1 (a), the sharp exothermic peaks near 130°C and 310°C are caused by the loss of crystalline water and the reaction of nitrate with citric acid, respectively. The reaction emits

a large amount of CO_2 and H_2O, which corresponds to the sharp reduction of weight on the TG curve. The exothermic peak after 600 °C is caused by the oxidation of residual carbon [18,36]. From Fig. 1 (b), the total weight loss in the test temperature range is 2.3% after ashing. This shows that ashing is very thorough.

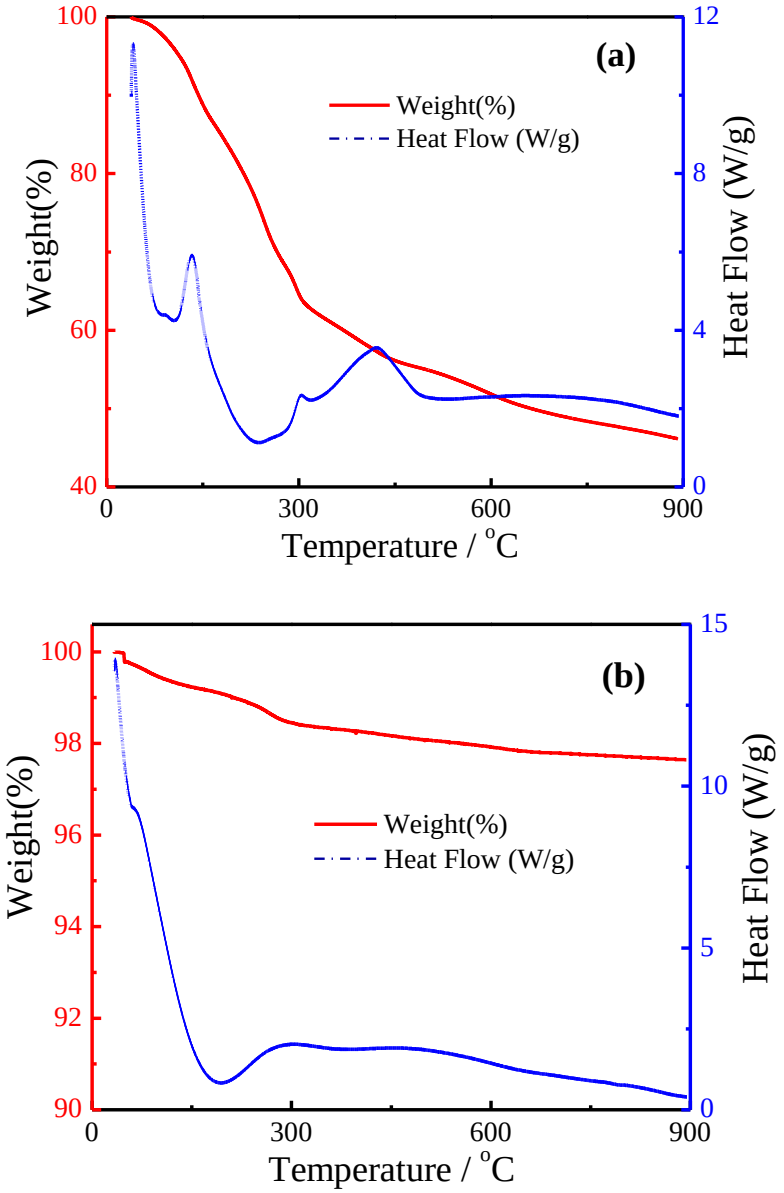

Figure 1. TG-DSC curve of the $Ce_{0.8}Gd_{0.2}O_{2-\alpha}$ gel from room temperature to 900 °C (a) before and (b) after ashing.

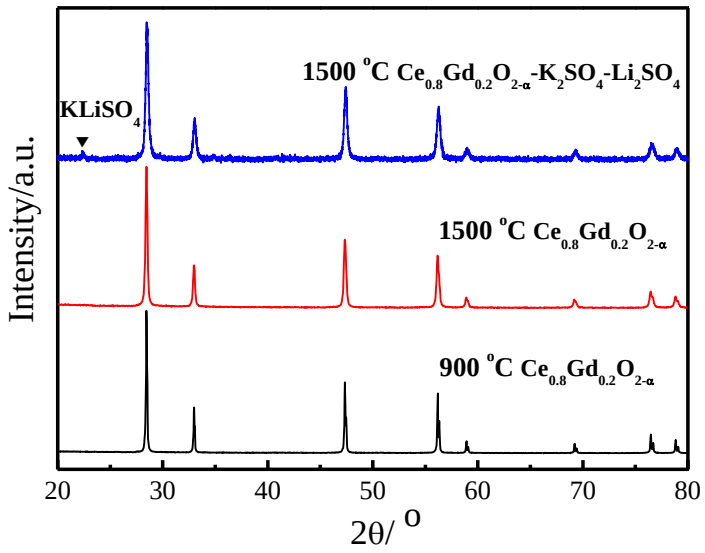

Figure 2. XRD spectra of $Ce_{0.8}Gd_{0.2}O_{2-\alpha}$ (900 °C, 1500 °C) and $Ce_{0.8}Gd_{0.2}O_{2-\alpha}$-$K_2SO_4$-$Li_2SO_4$.

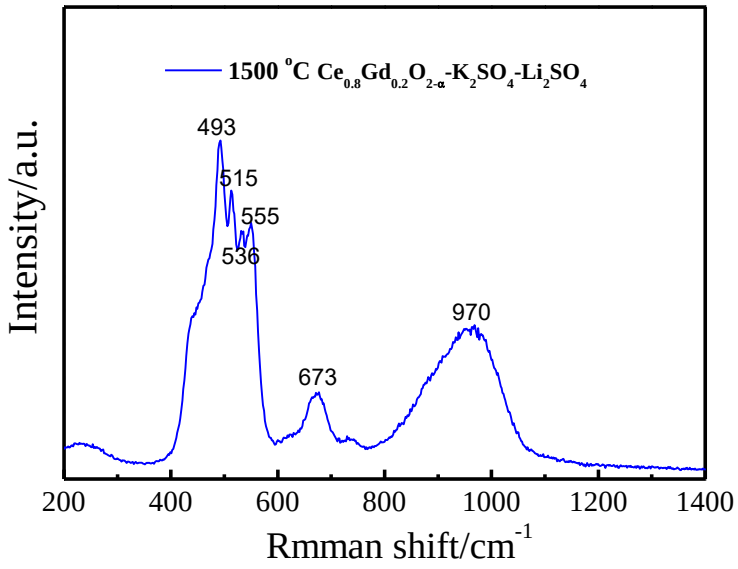

Figure 3. Raman spectrum of $Ce_{0.8}Gd_{0.2}O_{2-\alpha}$-$K_2SO_4$-$Li_2SO_4$.

The X-ray diffraction spectra of $Ce_{0.8}Gd_{0.2}O_{2-\alpha}$ (900 °C, 1500 °C) and $Ce_{0.8}Gd_{0.2}O_{2-\alpha}$-$K_2SO_4$-$Li_2SO_4$ are shown in Fig. 2. According to the characteristic peaks of XRD, the $Ce_{0.8}Gd_{0.2}O_{2-\alpha}$ (900 °C, 1500 °C) are a cubic fluorite structure of CeO_2, which indicates that the samples prepared by the sol-gel method have good phase formation [18-22]. In addition to CeO_2 phase, a small amount of $KLiSO_4$ phase exists in the $Ce_{0.8}Gd_{0.2}O_{2-\alpha}$-$K_2SO_4$-$Li_2SO_4$ sample. Maybe this is because K_2SO_4-Li_2SO_4 is in melt state during heat treatment. When the composite electrolyte powders are cooled from heating state to room temperature, most of the molten sulphates do not crystallize and are cooled to room temperature in an amorphous state. Therefore, there are only weak peaks of $KLiSO_4$ in the XRD spectrum. XRD spectra show that the $Ce_{0.8}Gd_{0.2}O_{2-\alpha}$ structure is not affected by K_2SO_4-Li_2SO_4, which means that it has good corrosion resistance to molten sulphates [28-34].

The Raman spectrum of $Ce_{0.8}Gd_{0.2}O_{2-\alpha}$-$K_2SO_4$-$Li_2SO_4$ is shown in Fig. 3. At 493 cm^{-1}, there is a strong Raman activity peak in the F_{2g} mode of Ce-O-Ce symmetrical stretching vibration. The Raman peaks around 536 cm^{-1} correspond to the S-O bending deformation vibration. The Raman peak at 673 cm^{-1} corresponds to O_h vibrational mode. The Raman peaks near 987 cm^{-1} are attributed to the S-O symmetrical telescopic vibration [37-39]. It can be seen that the prepared $Ce_{0.8}Gd_{0.2}O_{2-\alpha}$-$K_2SO_4$-$Li_2SO_4$ has a cubic structure of CeO_2 and the existence of SO_4^{2-}, which is consistent with Fig. 2.

Fig. 4 shows the SEM photos of $Ce_{0.8}Gd_{0.2}O_{2-\alpha}$ (1500 °C) and $Ce_{0.8}Gd_{0.2}O_{2-\alpha}$-$K_2SO_4$-$Li_2SO_4$. It can be seen from Fig. 4(a) that $Ce_{0.8}Gd_{0.2}O_{2-\alpha}$ (1500 °C) has basically reached dense sintering. Fig. 4(b) shows some holes, which are proved to be closed stomata by experiment. Fig. 4(c,d) show that composite electrolyte is aggregate formed by amorphous sulphate particles covering $Ce_{0.8}Gd_{0.2}O_{2-\alpha}$ powders, which is conducive to the formation of a continuous two-phase interface [32-34].

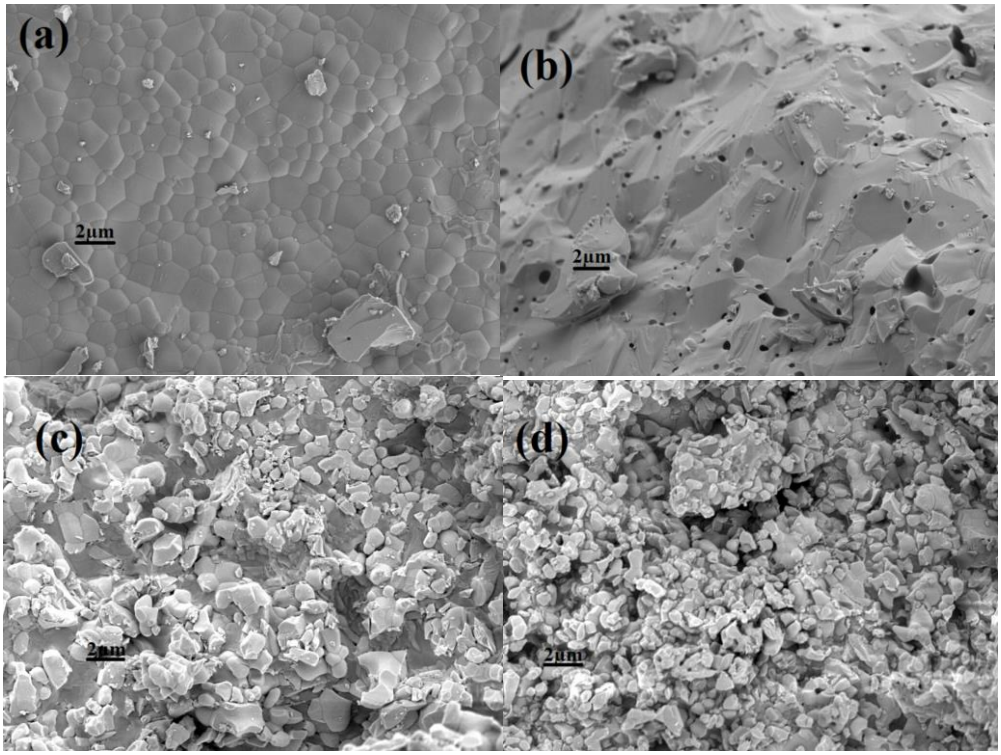

Figure 4. The external (a, c) and cross-sectional (b, d) SEM photos of $Ce_{0.8}Gd_{0.2}O_{2-\alpha}$ (1500 °C) and $Ce_{0.8}Gd_{0.2}O_{2-\alpha}$-$K_2SO_4$-$Li_2SO_4$.

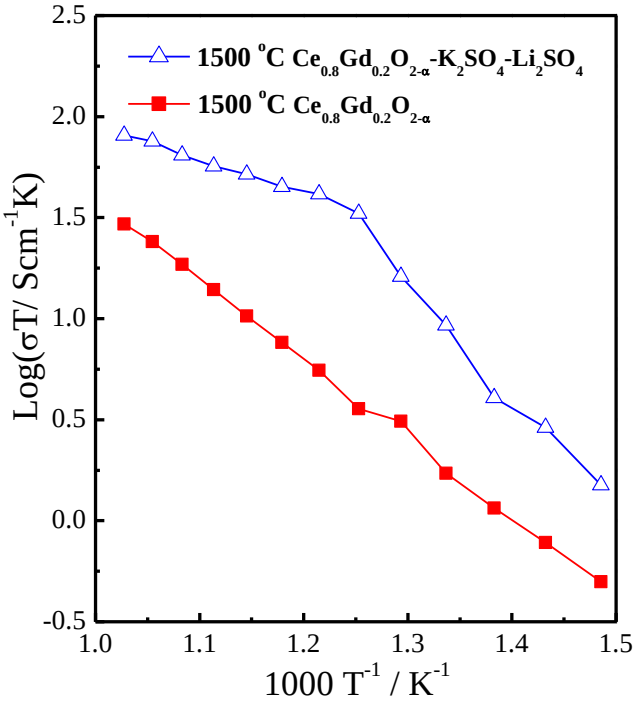

Figure 5. Arrhenius curves of $Ce_{0.8}Gd_{0.2}O_{2-\alpha}$ (1500 °C) and $Ce_{0.8}Gd_{0.2}O_{2-\alpha}$-$K_2SO_4$-$Li_2SO_4$ at 400- 700 °C.

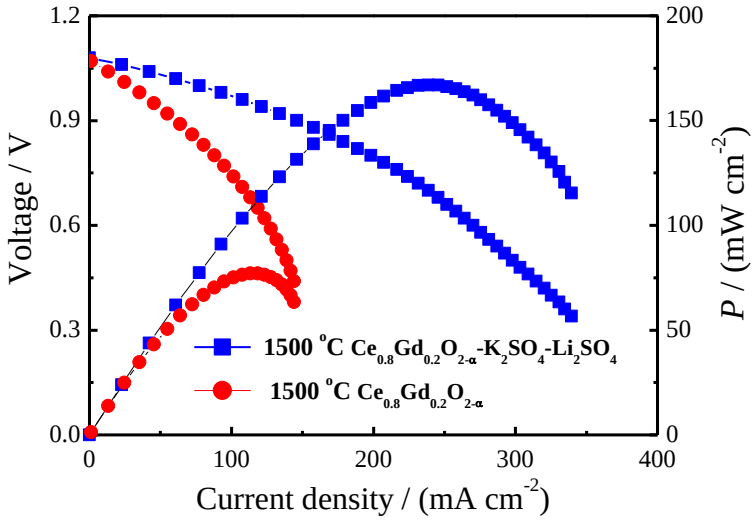

Figure 6. Volt-ampere characteristic curves of $Ce_{0.8}Gd_{0.2}O_{2-\alpha}$ (1500 °C) and $Ce_{0.8}Gd_{0.2}O_{2-\alpha}$-$K_2SO_4$-$Li_2SO_4$ at 700 °C.

Fig. 5 shows the Arrhenius curves of $Ce_{0.8}Gd_{0.2}O_{2-\alpha}$ (1500 °C) and $Ce_{0.8}Gd_{0.2}O_{2-\alpha}$-$K_2SO_4$-$Li_2SO_4$ in nitrogen at 400-700 °C. The Arrhenius curve of $Ce_{0.8}Gd_{0.2}O_{2-\alpha}$-$K_2SO_4$-$Li_2SO_4$ has a turning point where the conductivity transits near the temperature of 525 °C. The enhancement effect of conductivity is caused by the interface between two phases. Below the transition temperature, sulphate is solid phase with low conductivity. Ions are mainly transported through the interface and bulk of $Ce_{0.8}Gd_{0.2}O_{2-\alpha}$. With the increase of temperature, the melting process of sulphate begins to extend from the interface region to bulk phase. Above the transition temperature, the sulphate in the interface region begins to melt, which

is conducive to the conduction of ion defects through the interface region. The maximum conductivity of $Ce_{0.8}Gd_{0.2}O_{2-\alpha}$-$K_2SO_4$-$Li_2SO_4$ reaches 8.3×10^{-2} S·cm^{-1} at 700 °C [32-35, 40].

Fig. 6 shows the output performance of $Ce_{0.8}Gd_{0.2}O_{2-\alpha}$ (1500 °C) and $Ce_{0.8}Gd_{0.2}O_{2-\alpha}$-$K_2SO_4$-$Li_2SO_4$ at 700 °C. Open circuit voltages of $Ce_{0.8}Gd_{0.2}O_{2-\alpha}$ (1500 °C) and $Ce_{0.8}Gd_{0.2}O_{2-\alpha}$-$K_2SO_4$-$Li_2SO_4$ are higher than 1.05V. This shows that adding a certain amount of sulphate can effectively inhibit the electronic conductivity of $Ce_{0.8}Gd_{0.2}O_{2-\alpha}$. It also can be seen that the output power densities increase with the increase of current densities. The maximum output power densities of $Ce_{0.8}Er_{0.2}O_{2-\alpha}$ and $Ce_{0.8}Gd_{0.2}O_{2-\alpha}$-$K_2SO_4$-$Li_2SO_4$ are 77 mW·cm^{-2} and 167 mW·cm^{-2} at 700 °C, respectively [41-43]. The good fuel cell performance of $Ce_{0.8}Gd_{0.2}O_{2-\alpha}$-$K_2SO_4$-$Li_2SO_4$ is mainly attributed to the high ionic conductivity of composite electrolyte.

4. CONCLUSIONS

In this study, $Ce_{0.8}Gd_{0.2}O_{2-\alpha}$-$K_2SO_4$-$Li_2SO_4$ composite electrolyte was prepared by mixing $Ce_{0.8}Gd_{0.2}O_{2-\alpha}$ powder with binary sulphates. XRD shows $Ce_{0.8}Gd_{0.2}O_{2-\alpha}$ is a cubic fluorite structure of CeO_2 and it has good corrosion resistance to molten sulphates. The Raman spectrometer further indicates that $Ce_{0.8}Gd_{0.2}O_{2-\alpha}$-$K_2SO_4$-$Li_2SO_4$ has a cubic structure of CeO_2 and the existence of SO_4^{2-}. SEM shows that composite electrolyte is aggregate formed into a continuous two-phase interface. The maximum output power densities of $Ce_{0.8}Er_{0.2}O_{2-\alpha}$ and $Ce_{0.8}Gd_{0.2}O_{2-\alpha}$-$K_2SO_4$-$Li_2SO_4$ are 77 mW·cm^{-2} and 167 mW·cm^{-2} at 700 °C, respectively.

ACKNOWLEDGEMENTS

This work was supported by the National Natural Science Foundation (No. 51402052) of China, The Natural Science Project of Anhui Province (No. KJ2018A0337, KJ2019A0545, KJ2019A0539), Excellent Youth Foundation of Anhui Educational Committee (No. gxyq2018046), Horizontal cooperation project of Fuyang municipal government and Fuyang Normal University (No. XDHXTD201704, HX2019004000), Key School-level Youth Talent Foundation Program of Fuyang Normal University (2017rcxm15), School-level Natural Science Research Program of Fuyang Normal University (2018FSKJ18).

References

1. G. L. Liu, W. Liu, Q. Kou and S. J. Xiao, *Int. J. Electrochem. Sci*., 13 (2018) 2641.
2. T. Hibino, K. Kobayashi, P. Lv, M. Nagao, S. Teranishi and T. Mori, *J. Electrochem. Soc.*, 164 (2017) F557.
3. J. Cao, Y. Ji, X. Huang, H. Jia and W. Liu, *Ceram. Int.*, 44 (2018) 13602.
4. T. Hibino, K. Kobayashi, M. Nagao and S. Teranishi, *ChemElectroChem*, 4 (2017) 3032.
5. Y. Tian, Z. Lü, X. Guo and P. Wu, *Int. J. Electrochem. Sci*., 14 (2019) 1093.
6. C. Bernuy-Lopez, L. Rioja-Monllor, T. Nakamura, S. Ricote, R. O'Hayre, K. Amezawa, M. Einarsrud and T. Grande, *Materials*, 11 (2018) 196.
7. L. Bi, S. Boulfrad and E. Traversa, *Chem. Soc. Rev.*, 43 (2014) 8255.
8. T. Hibino, K. Kobayashi, P. Lv, M. Nagao and S. Teranishi, *Bull. Chem. Soc. Jpn.*, 90 (2017) 1017.

9. J. Luo, A.H. Jensen, N.R. Brooks, J. Sniekers, M. Knipper, D. Aili, Q. Li, B. Vanroy, M. Wübbenhorst, F. Yan, L.V. Meervelt, Z. Shao, J. Fang, Z.-H. Luo, D.E.D. Vos, K. Binnemans and J. Fransaer, *Energy Environ. Sci.*, 8 (2015) 1276.
10. Y. N. Chen, T. Tian, Z. H. Wan, F. Wu, J. T. Tan and M. Pan, *Int. J. Electrochem. Sci.*, 13 (2018) 3827.
11. A.A. Solovyev, S.V. Rabotkin, A.V. Shipilova and I.V. Ionov, *Int. J. Electrochem. Sci*., 14 (2019) 575.
12. J. Li, H. Zhang, M. Gao, Q. Li, W. Bian, T. Tao and H. Zhang, *Materials*, 11 (2018) 749.
13. M. A. Haque, A. B. Sulong, E. H. Majlan, K. S. Loh, T. Husaini and R. Rosli, *Int. J. Electrochem. Sci*., 14 (2019) 371.
14. D.-K. Lim, J.-H. Kim, A.U. Chavan, T.-R. Lee, Y.-S. Yoo and S.-J. Song, *Ceram. Int.*, 42 (2016) 3776.
15. X. Fang, J. Zhu and Z. Lin, *Energies*, 11 (2018) 1735.
16. M.S. Arshad, R. Raza, M.A. Ahmad, G. Abbas, A. Ali, A. Rafique, M.K. Ullah, S. Rauf, M.I. Asghar, N. Mushtaq, S. Atiq and S. Naseem, *Ceram. Int.*, 44 (2018) 170.
17. A. Maheshwari and H.-D. Wiemhöfer, *Ceram. Int.*, 41 (2015) 9122.
18. M.R. Kosinski and R.T. Baker, *J. Power Sources*, 196 (2011) 2498.
19. F. Altaf, R. Batool, R. Gill, G. Abbas, R. Raza, Z. Rehman and M.A. Ahmad, *Ceram. Int.*, 45 (2019) 10330.
20. M. Anwar, Muhammed Ali S.A., A. Muchtar and M.R. Somalu, *Ceram. Int.*, 45 (2019) 5627.
21. M. Kumar, J.-H. Yun, V. Bhatt, B. Singh, J. Kim, J.-S. Kim, B.S. Kim and C.Y. Lee, *Electrochim. Acta*, 284 (2018) 709.
22. T. Liu, X. Yang, C. Ma, X. Hao, X. Liang, F. Liu, F. Liu, C. Yang, H. Zhu and G. Lu, *Solid State Ionics*, 317 (2018) 53.
23. T. Petrisor Jr, A. Meledin, A. Boulle, R.B. Mos, M.S. Gabor, L. Ciontea and T. Petrisor, *Appl. Surf. Sci.*, 433 (2018) 668.
24. B.C. Yang, D. Go, S. Oh, J.W. Shin, H.J. Kim and J. An, *Appl. Surf. Sci.*, 473 (2019) 102.
25. Diaz-Aburto, F. Gracia and M. Colet-Lagrille, *Fuel Cells*, 19 (2019) 147.
26. T. Liu, W. Li, Y. Zhang, X. Hao, Y. Zhang, X. Liang, F. Liu, F. Liu, X. Yan, Y. Gao, T. Zhang, C. Zhang and G. Lu, *Sensor. Actuat. B. Chem.*, 284 (2019)751.
27. M. Anwar, S.A.M. Ali, A. Muchtar and M.R. Somalu, *J. Alloy. Compound.*, 775 (2019) 571.
28. A.I.B. Rondao, S.G. Patricio, F.M.L. Figueiredo and F.M.B. Marques, *Int. J. Hydrogen Energ.*, 39 (2014) 5460.
29. S. Shawuti and M.A. Gulgun, *J. Power Sources*, 267 (2014) 128.
30. B. Zhu, S. Li and B.E. Mellander, *Electrochem. Commun.*, 10 (2008) 302.
31. H. Sun, X. Guo, F. Yu, Z. Yang, G. Li, J. Li, H. Ding, F. Meng, Z. Fan, P. Wang, W. Yan and Z. Hu, *Ceram. Int.*, 45 (2019) 7667.
32. J.T. Kim, T.H. Lee, K.Y. Park, Y. Seo, K.B. Kim, S.J. Song, B. Park and J.Y. Park, *J. Power Sources*, 275 (2015) 563.
33. G. Zhang, W. Li, W. Huang, Z. Cao, K. Shao, F. Li, C. Tang, C. Li, C. He, Q. Zhang and L. Fan, *J. Power Sources*, 386 (2018) 56.
34. Q.X. Fu, S.W. Zha, W. Zhang, D.K. Peng, G.Y. Meng and B. Zhu, *J. Power Sources*, 104 (2002) 73.
35. C. Slim, L. Baklouti, M. Cassir and A. Ringuedé, *Electrochim. Acta*, 123 (2014) 127.
36. M.T. Soo, N. Prastomo, A. Matsuda, G. Kawamura, H. Muto, A.F.M. Noor, Z. Lockman and K.Y. Cheong, *Appl. Surf. Sci.*, 258 (2012) 5250.
37. S. Phokha, S. Hunpratub, B. Usher, A. Pimsawat, N. Chanlek and S. Maensiri, *Appl. Surf. Sci.*, 446 (2018) 36.
38. S. Preethi, M. Abhiroop and K.S. Babu, *Ceram. Int.*, 45 (2019) 5819.
39. M.A. Rodrigues, A.C. Catto, E. Longo, E. Nossol and R.C. Lima, *J. Rare Earth.*, 36 (2018) 1074.

40. A. Rafique, R. Raza, N.A. Arifin, M.K. Ullah, A. Ali and R. Steinberger-Wilckens, *Ceram. Int.*, 44 (2018) 6493.
41. S. Kobi, N. Jaiswal, D. Kumar and O. Parkash, *J. Alloy Compd.*, 658 (2016) 513.
42. J. Ma, N. Duan, Y. Han, D. Yan, B. Chi, J. Pu and J. Li, *J. Power Sources*, 401 (2018) 397.
43. S.S.B.C. Abdullah, T. Teranishi, H. Hayashi and A. Kishimoto, *J. Power Sources*, 374 (2018) 92.